A study on impact of pre-processing in Hartmann-Shack Wavefront Sensing

A Project Report

submitted by

T. CHANDRAHAS

in partial fulfilment of the requirements
for the award of the degree of

BACHELOR OF TECHNOLOGY

DEPARTMENT OF ELECTRICAL ENGINEERING
INDIAN INSTITUTE OF TECHNOLOGY, MADRAS.

June 2016

THESIS CERTIFICATE

This is to certify that the thesis entitled **A study on impact of pre-processing in Hartmann-Shack Wavefront Sensing**, submitted by **T. Chandrahas**, to the Indian Institute of Technology Madras, for the award of the degree of **Bachelor of Technology**, is a bona fide record of the work carried out by him under the supervision of Prof. Vasudevan Lakshminarayanan, School of Optometry and Vision Sciences, University of Waterloo, Canada. The contents of this thesis, in full or in parts, have not been submitted to any other Institute or University for the award of any degree or diploma.

Dr. Shanti Bhattacharya
Project Co-Guide
Associate Professor
Dept. of Electrical Engineering
IIT Madras, 600 036

Place: Chennai

Date: 10th June, 2016

ACKNOWLEDGEMENTS

I would like to express my deepest gratitude to Prof. Vasudevan Lakshminarayanan from University of Waterloo, for the opportunity to work on this project. His constant support, encouragement and constructive feedback while working on this project definitely helped me deliver my best in this work.

I am greatly thankful to Abbas Ommani for going to all lengths to help me in understanding the hardware better and for all the time he had spent in assisting me with the data acquisition. Without his enthusiasm and active involvement this would not have been possible. I am also thankful to Ritambar Burman and Dambar Thapa, the discussions I had with them gave me valuable insights during various stages of this project.

Further, I would like to thank my family members who have been a great source of inspiration and strength throughout my life. I am indebted to them for providing me with the opportunities when it mattered the most.

I am grateful to Prof. Shanti Bhattacharya and Prof. Harishankar Ramachandran, who were very accommodating in the last moment and made it possible for me to present this work as my undergraduate project.

ABSTRACT

KEYWORDS: Aberrometer, Hartmann Shack Wavefront Sensor (HSWS), Centroid Estimation

Hartmann-Shack Wavefront Sensor (HSWS) is an optical instrument used for characterizing an optical/imaging system. It is commonly used to estimate the optical wave front aberrations by measuring the distorted wave front. The accuracy of the estimation of optical aberrations using a Hartmann-Shack wavefront sensor (HSWS) is mainly dependent upon the measurement accuracy of the centroid of the focal spot. Centroid estimation is sensitive to the influence of reflections, scattered light, and noise; especially in the case where the signal spot area is smaller compared to the whole sub-aperture area. Instead of developing complex centroiding algorithms to mitigate these effects, the possibility of using a pre-processing routine is explored in this study. A comparison of performance of the commonly used centroiding methods on estimation of optical aberrations, with and without the use of some pre-processing steps (thresholding, Gaussian smoothing and adaptive windowing) is given. As an example the aberrations of the human eye model are used. This is done using the raw data collected from a custom made ophthalmic aberrometer and a model eye to emulate myopic and hypermetropic defocus values up to 2 Diopters. It is found that the use of any simple centroiding algorithm is sufficient in the case of ophthalmic applications for estimating aberrations within the typical clinically acceptable limits of a quarter Diopter margins, when certain pre-processing steps to reduce the impact of external factors are used.

TABLE OF CONTENTS

LIST OF TABLES

LIST OF FIGURES

ABBREVIATIONS

HSWS	Hartmann-Shack Wavefront Sensor
BSC	Brightest Spot Center
CoM	Center of Mass
WCoG	Weighted Center of Gravity
ICoG	Intensity Weighted Center of Gravity

CHAPTER 1

INTRODUCTION

Retinal imaging systems capture a digital image of the retina and help in early detection and management of several diseases like Glaucoma. In order to accurately capture the image of the retina, the optical wavefront distortions caused by the eye need to be taken into account (measured using Hartmann Shack Aberrometer) and compensated for using adaptive optics. The optics of the eye is not perfect and, to achieve diffraction limited resolution, aberrations must be corrected. Ocular aberrations have an explicit effect on the retinal image quality. Interaction of light with ocular tissue whether it is light scattered by the retina or by other ocular structures such as the cornea and the crystalline lens further degrades the quality of the retinal image. Wavefront aberrations describe the optical imperfections of the eye by measuring the complete refractive elements of the eye.

A wave front sensor is a device that is used to measure the optical wave front aberration and the Hartmann-Shack Wave front Sensor (HSWS) is the most commonly used optical wave front sensor. It uses an array of identical micro lenses and a detector which is placed at the focal plane of the micro lenses. When a plane wave front is incident on the HSWS, a pattern of equidistant focal spots is observed at the detector plane. Any deviation in the wave front as seen in Figure 1.2, imparts a displacement of the HS spots from their original (planar) positions. The horizontal and vertical displacements correspond to information of the local wave front slopes of the distorted wave front. The shift in the focal centers of the spots is used to measure the distorted wave front and thus estimate the aberrations

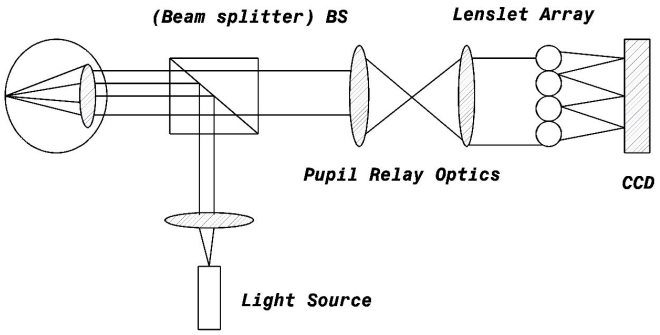

Figure 1.1: Hartmann Shack Wavefront Sensor Layout

in the eye. As noted by Leroux and Dainty (2010), the estimation of centroids of the HS spots corresponds to the largest reduction in data during the measurement procedure.

Since the accuracy of wave front reconstruction hinges on the accuracy of centroid estimation, it is a very crucial step. Practical setups of aberrometers are affected by different types of noise e.g., photon noise, readout noise and speckle noise that makes centroid estimation difficult (Diaz-Santana, 2015). A simple way to estimate the centroid is by picking the brightest pixel from the focal spot (Burman *et al.*, 2015).The more common way to find the centroid is to use the first image moment or the center of mass of entire sub-apertures of the individual micro lenses. However, these processes of centroid estimation are sensitive to external factors such as reflections, scattered light, and noise, particularly in the case when the signal spot area is smaller compared to the whole sub-aperture area (Xia and Ma, 2010).

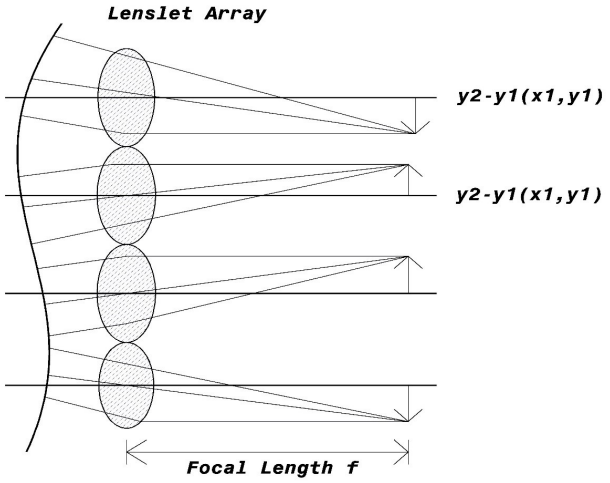

Figure 1.2: Displacement caused by an aberrated waveform. This images shows displacement along y axis. Similarly there is a shift along x axis also.

1.1 Centroiding Methods:

The focal center of each HS spot can be estimated in several ways. Some of the commonly used techniques are listed below.

1.1.1 Brightest Spot Center (BSC):

This is one of the elementary ways to estimate the centroid location in the focal spot. The brightest pixel or the pixel with the highest intensity in the focal spot corresponds to the centroid of the focal spot. Since in most cases the focal spot has a Gaussian like intensity distribution around the centroid, this can be used to locate the centroid. This works best when the noise has a lower intensity profile and the peak noise intensity is less than the peak signal intensity.

1.1.2 First image moment (Center of Mass - CoM):

The first image moment method or the center of mass (CoM) calculates the centroid location as the weighted mean of the position coordinates (xc, yc), the weight being the spot intensity as a function of position coordinates (x, y). The centroid, of a single sub-aperture spot pattern is evaluated using:

$$(x_c, y_c) = \left(\frac{\Sigma(I(x,y) \times x)}{\Sigma(I(x,y))}, \frac{\Sigma(I(x,y) \times y)}{\Sigma(I(x,y)} \right)$$

where xc and yc denote the centroid locations along the x and y coordinate axes, and I(x, y) denote the intensity of the pixel located at (x, y) and x and y denote the location of the pixel. This is one of the most widely used methods of centroid estimation and is best suited to situations where the light intensity levels are sufficiently high and the signal to noise ratio (SNR) is good. This method is highly sensitive to noise.

1.1.3 Weighted center of gravity (WCoG):

The mathematical form that is assumed for the shape of the spot is called the weighting function W(x, y), and is multiplied with the intensity function before applying the center of mass algorithm as previously discussed. The estimated centroid location becomes:

$$(x_c, y_c) = \left(\frac{\Sigma(W(x,y) \times I(x,y) \times x)}{\Sigma(W(x,y) \times I(x,y))}, \frac{\Sigma(W(x,y) \times I(x,y) \times y)}{\Sigma(W(x,y) \times I(x,y))} \right)$$

In this case, W(x, y), the weighting function is chosen to be a Gaussian kernel

so that, the scattered noise around the peripheries does not affect the estimation of the centroid position.

1.1.4 Intensity weighted center of gravity (ICoG):

Intensity weighted center of gravity (ICoG) is similar to WCoG with the difference being that the weighting function, W is a power of the intensity distribution of the spot pattern, I. Hence, in ICoG, the estimated centroid position becomes:

$$(x_c, y_c) = \left(\frac{\Sigma(I(x,y)^{\alpha} \times x)}{\Sigma(I(x,y)^{\alpha})}, \frac{\Sigma(I(x,y)^{\alpha} \times y)}{\Sigma(I(x,y)^{\alpha}} \right)$$

α determines the weighting given to intensity and a higher power of alpha implies greater importance to high intensity pixels. A value of 3 for alpha is used in this analysis following the work by Baik *et al.* (2007). In comparison to the CoM method, this algorithm should perform better under low light level conditions, and low background and readout noise as it gives greater priority for high intensity spots, and is less sensitive to the low intensity speckled noise due to reflections and diffraction prominent around the peripheries.

Statistical algorithms for centroid estimation tend to offer reasonable sub-pixel accuracy while being computationally less intensive.

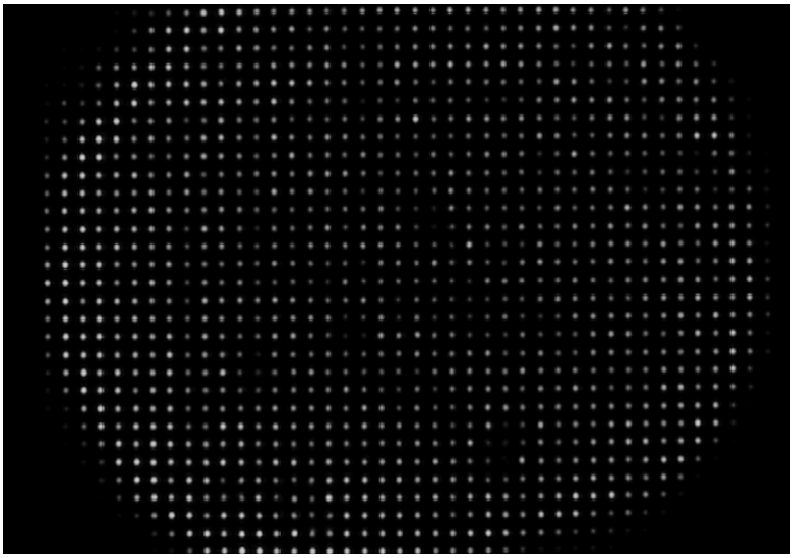

Figure 1.3: Hartmann Shack spot pattern

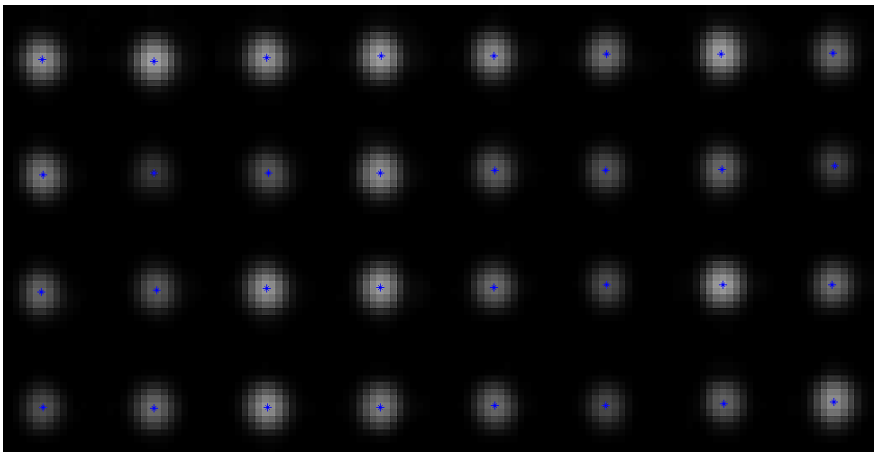

Figure 1.4: Estimated centroids for the Hartmann Shack spots

1.2 Pre-Processing Routine Used:

1.2.1 Averaging:

The aberrometer records data at a rate of at least 24 frames per second. These frames are then averaged to improve the accuracy of the system by reducing the speckle noise.

1.2.2 Intensity thresholding:

The gray scale images are first subjected to thresholding with respect to intensity. To keep the time complexity small without degrading the accuracy, the grayscale images are subjected to one-level hard thresholding expressed as a percentage of peak intensity in the image. The threshold depends on the illumination of the image as well as several other factors like quality of the image. If there is some reflection on the HS image such that the spots become blurry with slightly illuminated regions outside the HS spot edges, the threshold needs to be on the higher side. Similarly, the threshold needs to be lowered if the overall image is dull with lower illuminations. Anything above the threshold intensity is treated as a valid focal spot.

1.2.3 Spot size thresholding:

Each focal spot is a cluster of certain number of pixels. Another threshold with respect to number of connected pixels forming the spot is used. This re-classification of spots is to avoid noise being counted as a spot; each spot must have a minimum number of pixels that is specified by the user(Spiricon, 2004).

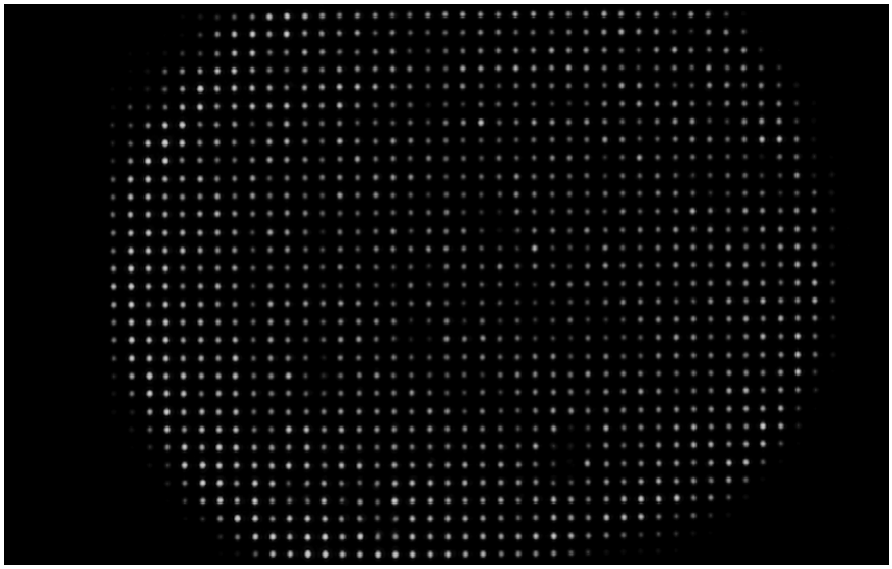

Figure 1.5: Raw Hartmann Shack spot pattern

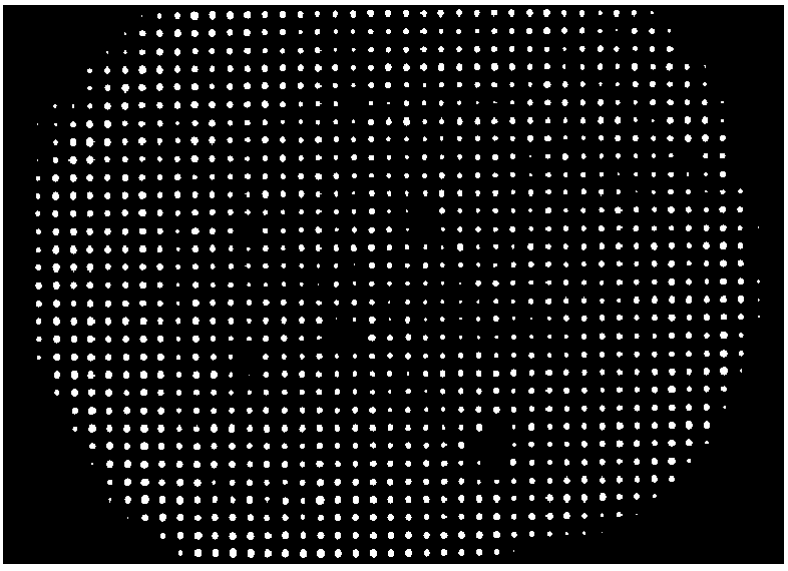

Figure 1.6: Hartmann Shack spot pattern after intensity thresholding with lower bound as 10 % of peak intensity

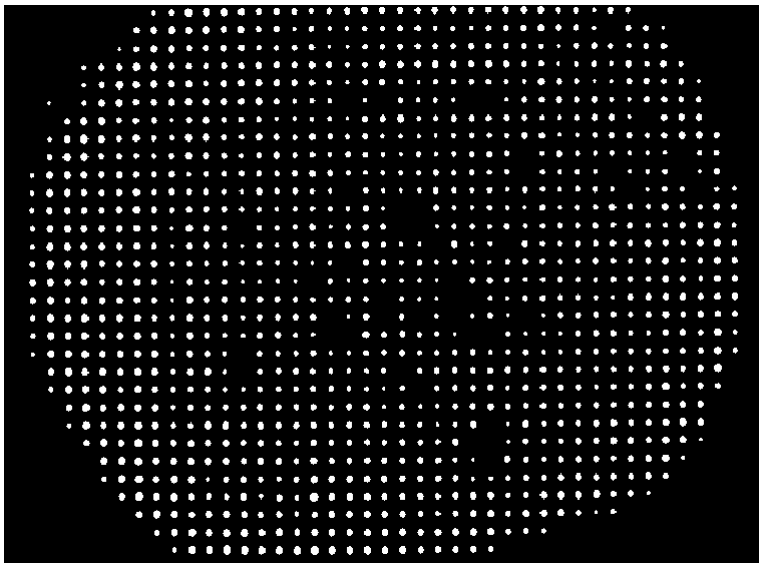

Figure 1.7: Hartmann Shack spot pattern after spot size thresholding to keep clusters which have more than 10 pixels

1.2.4 Gaussian Smoothing:

The input images are filtered using a Gaussian kernel. This is a process of blurring the image typically to reduce noise in the image. Mathematically, applying the Gaussian blur is the same as convolving the image with a Gaussian filter. This acts as a low pass filter and helps to reduce the effect of high frequency noise.

1.2.5 Adaptive Windowing:

In conventional methods, the whole sub-aperture is used as the detection window. When the noise spots are far from the focal spots or the intensity of the noise spots is stronger than that of the focal spots, the centroid accuracy is decreased by the noise. As described in Burman *et al.* (2015), the centroid was previously estimated using a fixed sub-aperture area calculated using the knowledge about the apparatus and the images. Instead of using the entire sub-aperture area of each lens let for estimating the centroid of the focal spot, the boundaries of all individual

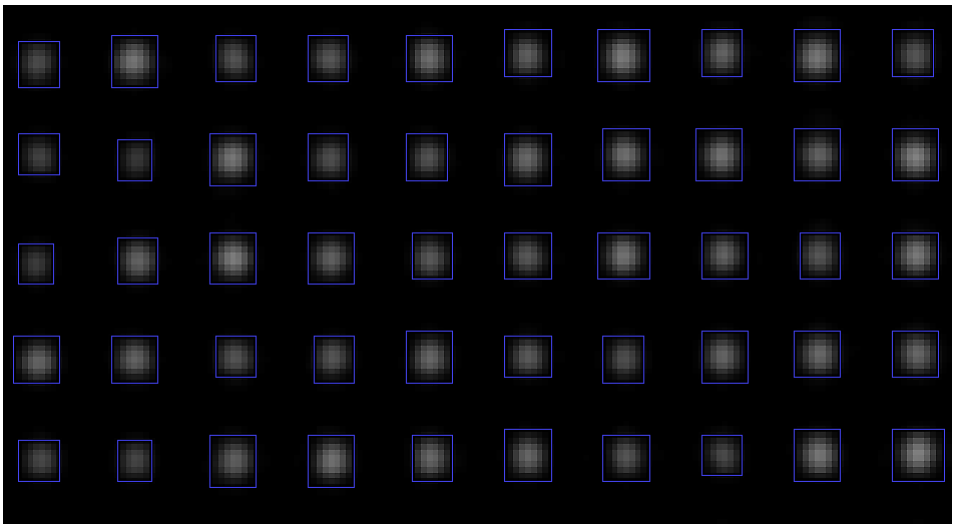

Figure 1.8: Hartmann Shack spot pattern showing the adaptive window around each spot

spots classified through thresholding are evaluated and used to define a dynamic rectangular boundary around each focal spot. The evaluation of centroid location is then processed only within this window, to reduce the effect of peripheral noise. This also helps reduce the processing required due to a smaller region of processing. In the next section we describe the measurement and analysis using experimental obtained data.

CHAPTER 2

Study of impact of the pre-processing routine on the centroiding performance of some common centroiding algorithms

Apparatus Used:

The apparatus (Figure 2.1) used for the experiment is a custom made aberrometer based on an original design by Diaz-Santana *et al.* (2007). Instead of a human eye, a model eye as seen in Figure 2.3, having a focal length of 130 mm, was used to simulate various refractive errors. As the reference, a flat plane mirror was used.

The light source is a laser diode (LD) with a wavelength of 780nm (5mW, circular beam, focusable, maximum 5mm diameter, 8-30 VDC). The lenslet array used is Thorlabs MLA150-5C (10 mm x 10 mm Lens Array, 300-1100 nm, Chrome Mask, Pitch=150 μm, f=5.2 mm). The beam from the source is spatially filtered to a beam width of 1mm or less, effectively limiting the proportion of the maximum power of the light source allowed to enter the instrument and, therefore, acting as a safety measure by preventing accidental exposure of the eye to the maximum power of the source. This is a necessary precautionary measure when the aberrometer is used on human subjects.

The apparatus is calibrated and then the data is collected. The data for each set included the images of the Hartmann Shack spots captured for simulated

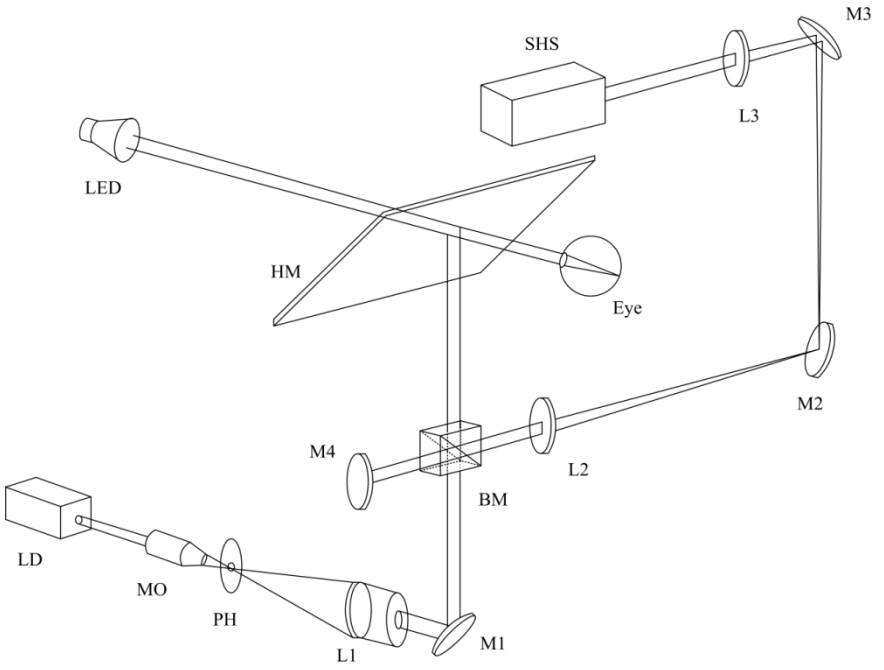

Figure 2.1: Schematic illustration of the optical setup: LD = laser diode; MO = microscope objective; PH = pinhole; L1, L2, and L3 = lenses; M1, M2, and M3 = mirrors; M4 = removable mirror used for calibration; BM = beam splitter; HM = viewing window (hot mirror); SHS = Shack-Hartmann sensor.

aberrations from - 2D to + 2D in intervals of 0.5D. Also a reference image is captured by use of a flat mirror to simulate a planar wave front. The aberrometer records data at a rate of at least 24 frames per second. These frames are then averaged to improve the accuracy of the system by reducing the speckle noise.

Procedure Followed to estimate optical aberrations:

This procedure followed in estimating the optical aberrations is explained below:

1. Let I(x, y) be the averaged subject image acquired using a model eye having 130 mm focal distance through the lens let array by the CCD detector and R be the averaged reference image acquired with a flat mirror. These images are first smoothed using a Gaussian filter (1.2.4) and then subjected to thresholding as described in 1.2.2 and 1.2.3 in order to classify the focal spots.
2. The boundary pixels of the above classified individual HS spots is then detected and used to form a bounding rectangle surrounding the spot as

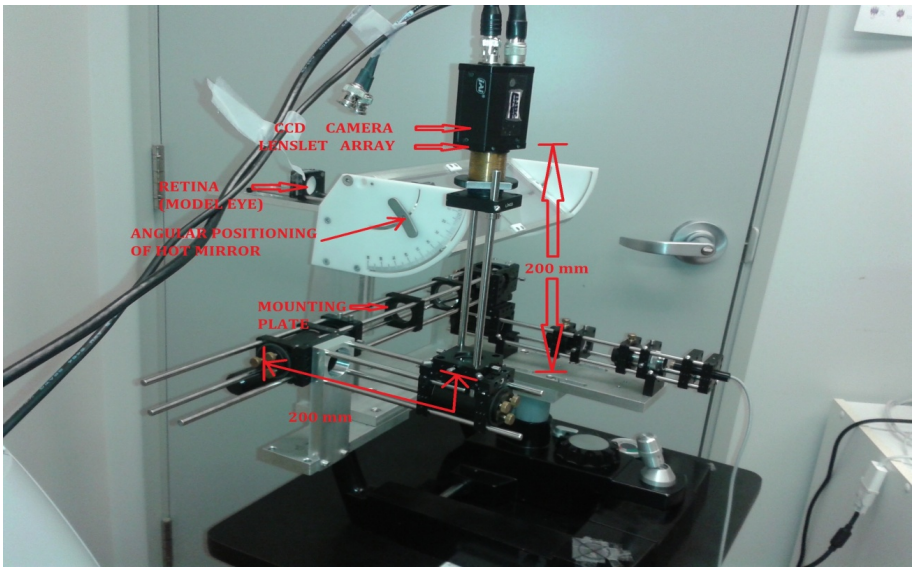

Figure 2.2: Setup of the apparatus

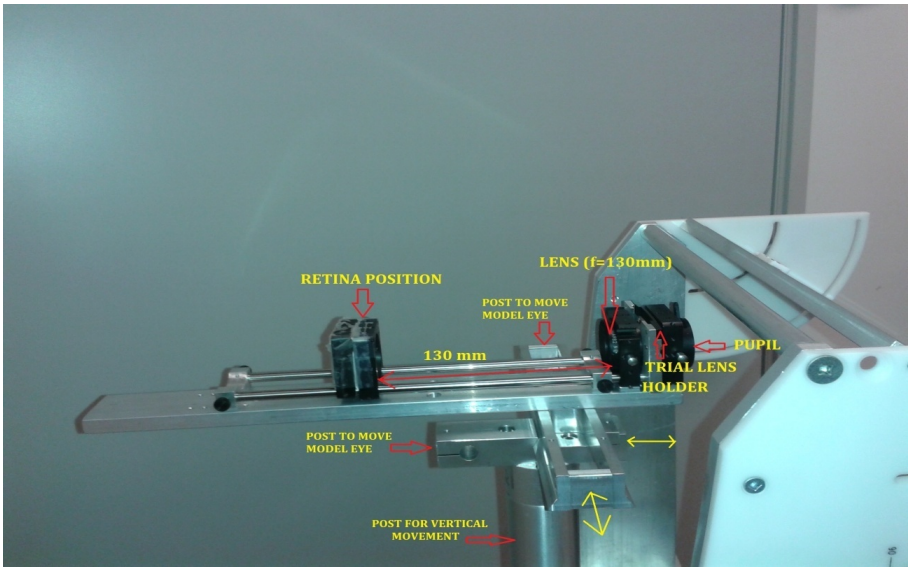

Figure 2.3: Setup of Model Eye

described in 1.2.5. This dynamic window is then used for estimating the centroids of the focal spots using the different methods of centroiding mentioned. Only the spots that lie within the effective pupil radius are used for further processing.

3. The shifts of the centroids of the subject image are calculated using the centroids of the reference image to give the local slopes of the wave front:

$$(m_{x_x}, m_{y_i}) = \left(\frac{\triangle x_i}{f}, \frac{\triangle y_i}{f}\right)$$

where f is the focal length of the lens let array, Δx_i and Δy_i denote the shifts in the focal spot along the x and y Cartesian coordinates.

4. The slopes of the wave front are then used to represent it in terms of Zernike polynomials (Lakshminarayanan and Fleck, 2011; Maeda, 2003):

$$(m_{x_x}, m_{y_i}) = \left(\sum_{n=0}^{\infty} C_n \frac{\partial \overline{Z_{nx}(x,y)}}{\partial x}, \sum_{n=0}^{\infty} C_n \frac{\partial \overline{Z_{nx}(x,y)}}{\partial y}\right)$$

where, the integration occurs over the pupil circle. C_n's are the Zernike coefficients. Z_n(x, y) are the Zernike polynomials.

5. The Zernike coefficients are calculated using the Least Squares Fit (LSF) method from the above equations. We need more equations than the coefficients being determined, which sets a minimum bound on the number of lenses in the lenslet array. So we need more than 20 lenslets (that capture as many focal spots) if we wish to estimate the first 20 Zernike coefficients. From the predicted coefficients the spherical defocus can be modeled as below which gives the result in DioptersMaeda (2003):

$$S = -\frac{4\sqrt{3}}{r^2}C_4 + \sqrt{\left(-\frac{2\sqrt{3}}{r^2}C_3\right)^2 + \left(-\frac{2\sqrt{3}}{r^2}C_5\right)^2}$$

where S denotes the spherical defocus and r denotes the pupil radius.

Experimental Results:

The HS images were obtained from the CCD sensor and stored in Macintosh computer using i-Movie 10.0 software. The images were processed following the outline mentioned above. The calculated spherical defocus values using the dif-

Table 2.1: Results using raw images.

Trial Lens Used (D)	BSC	CoM	WCoG	ICoG
-2	-1.67068	2.974606	3.680644	-1.58364
-1.5	-1.40202	-1.21031	-1.21066	-1.37229
-1	-0.95218	-0.67875	-0.65885	-0.71955
-0.5	-0.73624	-0.36703	-0.35451	-0.52972
0	-0.18463	0.379915	0.359663	-0.14618
0.5	0.238225	1.158279	0.972031	0.670321
1	0.920827	1.281183	1.124245	1.034609

Table 2.2: Results using pre-processed images.

Trial Lens Used (D)	BSC	CoM	WCoG	ICoG
-2	-1.75984	-1.79691	-1.79612	-1.78703
-1.5	-1.37061	-1.39965	-1.40219	-1.37846
-1	-1.03696	-1.07056	-1.0712	-1.0607
-0.5	-0.66854	-0.6699	-0.67009	-0.66979
0	-0.24491	-0.22147	-0.22093	-0.22119
0.5	0.251834	0.284788	0.284201	0.285978
1	0.861102	0.906341	0.909152	0.89675

ferent centroiding algorithms with and without use of the pre-processing methods are given below. Even though results for only the images with the complete pre-processing routine are given here, the intermediate results are discussed later. 2.1 gives the estimated spherical defocus when different centroiding methods are used on raw images for a particular set and 2.2 gives the estimated spherical defocus when different centroiding methods are used on pre-processed images for the same set.

Estimated spherical defocus of raw images, for higher values of defocus the spots are adversely affected, giving completely erroneous results with certain algorithms. This is because higher myopic defocus values blur out spots and spread them over larger areas causing the intensity values take a hit. Algorithms that give weightage to intensity perform better than other algorithms in that case and the intensity weighted center of gravity method is more robust amongst them.

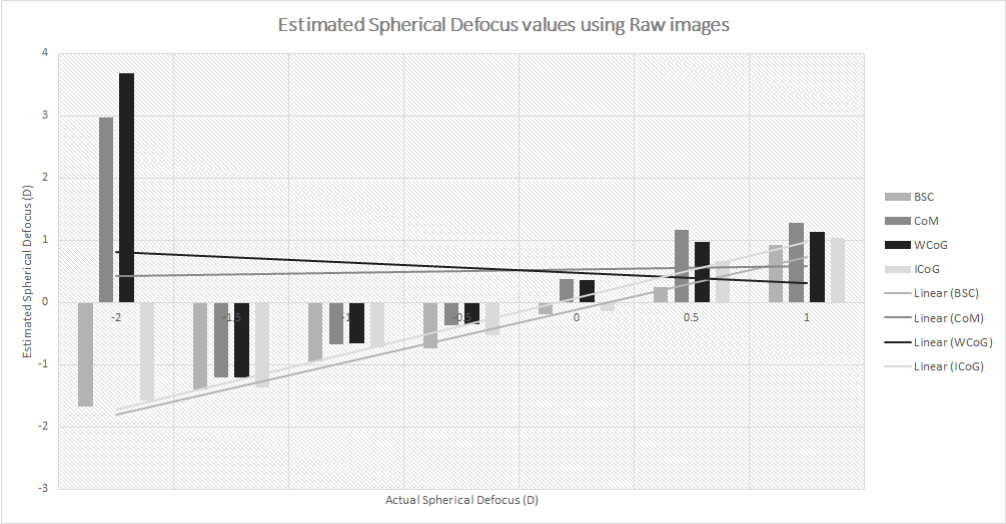

Figure 2.4: Plots of the spherical defocus results calculated using BSC, CoM, ICoG and WCoG respectively on images which have not been pre-processsed. Their respective linear trend lines have also been plotted.

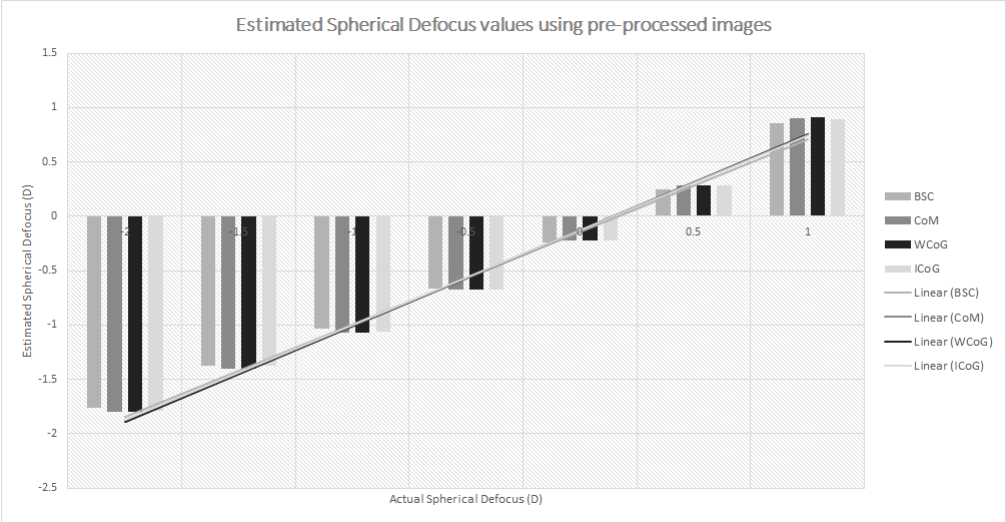

Figure 2.5: Plots of the spherical defocus results calculated using BSC, CoM, ICoG and WCoG respectively on pre-processed images. Their respective linear trend lines have also been plotted.

The above results show that the values calculated are within +/- 0.25D margin of the trial lens used when they were smoothed, thresholded and processed using a dynamic window. It can clearly be observed that by using these pre-processing routines the resulting outcomes from the use of different centroiding algorithms follow a close linear trend. It can also be seen that the use of the different centroiding algorithms, results in more or less the same estimate for the aberration, if the images are pre-processed.

The procedure was repeated for several data sets collected over time and the conclusions drawn are on basis of those results.

CHAPTER 3

Conclusions:

The pre-processing routine used helps improve the performance of the centroiding methods and makes the procedure more robust. The main step that results in a drastic improvement of the results is an appropriate thresholding step, making it the single most crucial pre-processing step. The adaptive windowing is to ensure that the processing area is minimized resulting in upto threefold faster processing. These pre-processing steps not only make the results more accurate but also help minimize the effect of external factors like reflections, scattered light and noise. The sensitiveness to external factors that affect different algorithms in different ways is minimized by use of the pre-processing routines, making it feasible to use any centroiding algorithm of choice.

In the case of ophthalmic applications, use of any simple centroiding algorithm seems to be sufficient for estimating aberrations within the typical clinically acceptable limits of a quarter Diopter margins, when the suggested pre – processing steps are used to mitigate the impact of external factors.

Publications

1. **C. Thatiparthi, A. Ommani, R. Burman, D. Thapa, N. Hutchings, & V. Lakshminarayanan**, "Comparison of performance of some common Hartmann-Shack centroid estimation methods", Proc. SPIE 9693, Ophthalmic Technologies XXVI, 969321 (2016), DOI: 10.1117/12.2219857

REFERENCES

Baik, S., **S. Park**, **C. Kim**, and **B. Cha** (2007). Estimation of centroid positions with a matched-filter algorithm: relevance for aberrometry of the eye. *Optics and Laser Technology*, **39(2)**, 262–267. 1.1.4

Burman, R., **A. Ommani**, **D. Thapa**, **K. Raahemifar**, **N. Hutchings**, and **V. Lakshminarayanan**, A method for estimating the wavefront aberrations with missing spot data in a shack-hartmann aberrometer. *In* **V. Lakshminarayanan** and **I. Bhattacharya** (eds.), *Advances in Optical Science and Engineering*. Springer, New Delhi, India, 2015. URL `http://dx.doi.org/10.1007/978-81-322-2367-2_40`. 1, 1.2.5

Diaz-Santana, L. (2015). *Wavefront sensing in the human eye with a Shack-Hartmann sensor*. Ph.D. thesis, Department of Physics - Imperial College London. 1

Diaz-Santana, L., **V. Gueriaux**, **G. Arden**, and **S. Gruppetta** (2007). New methodology to measure the dynamics of ocular wave front aberrations during small amplitude changes of accommodation. *Optics Express*, **15(9)**, 5649–5663. 2

Lakshminarayanan, V. and **A. Fleck** (2011). Zernike polynomials: a guide. *Journal of Modern Optics*, **58**, 545–561. 4

Leroux, C. and **C. Dainty** (2010). Estimation of centroid positions with a matched-filter algorithm: relevance for aberrometry of the eye. *Optics Express*, **18(2)**, 1197–1206. 1

Maeda, P. (2003). Zernike polynomials and their use in describing the wavefront aberrations of the human eye. Technical report, Stanford University. 4, 5

Spiricon, *Hartmann Wavefront Analyzer Tutorial*. Spiricon Inc., Logan, Utah, USA 84341, 2004. 1.2.3

Xia, A. and **C. Ma**, An improved centroid detection method based on higher moment for shack-hartmann wavefront sensor. *In* **T. Yoshizawa**, **P. Wei**, **J. Zheng**, and **T. Shimura** (eds.), *Optoelectronic Imaging and Multimedia Technology*. SPIE, Beijing, China, 2010. URL `http://dx.doi.org/10.1117/12.870136`. 1